Comparing quantum fluctuations in the spin-$\frac{1}{2}$ and spin-1 XXZ Heisenberg models on the square and honeycomb lattices

Masahiro Kadosawa,[1] Masaaki Nakamura,[2] Yukinori Ohta,[1] and Satoshi Nishimoto[3,4]

[1]*Department of Physics, Chiba University, Chiba 263-8522, Japan*

[2]*Department of Physics, Ehime University, Ehime 790-8577, Japan*

[3]*Department of Physics, Technical University Dresden, 01069 Dresden, Germany*

[4]*Institute for Theoretical Solid State Physics, IFW Dresden, 01069 Dresden, Germany*

(Received 11 April 2024; revised 2 July 2024; accepted 27 September 2024; published 10 October 2024)

We present a detailed investigation of the XXZ Heisenberg model for spin-1/2 and spin-1 systems on square and honeycomb lattices. Utilizing the density-matrix renormalization group method, complemented by spiral boundary conditions (SBCs) for mapping two-dimensional (2D) clusters onto one-dimensional chains, we meticulously explore the evolution of staggered magnetization and spin gaps across a broad spectrum of easy-axis anisotropies. Our study reveals that despite the lower site coordination number of the honeycomb lattice, which intuitively suggests increased quantum fluctuations in its Néel phase compared to the square lattice, the staggered magnetization in the honeycomb structure exhibits only a marginal reduction. Furthermore, our analysis demonstrates that the dependence of staggered magnetization on the XXZ anisotropy Δ, except in close proximity to $\Delta = 1$, aligns with series expansion predictions up to the 12th order. Notably, for the $S = 1/2$ honeycomb lattice, deviations from the 10th-order series expansion predictions near the isotropic Heisenberg limit emphasize the critical influence of quantum fluctuations on the spin excitation in its Néel state. Additionally, our findings are numerically consistent with the singular behavior of the spin gap near the isotropic Heisenberg limit as forecasted by spin-wave theory. The successful implementation of SBCs marks a methodological advancement, streamlining the computational complexity involved in analyzing 2D models and paving the way for more precise determinations of physical properties in complex lattice systems.

DOI: 10.1103/PhysRevB.110.134418

I. INTRODUCTION

In the complex world of quantum magnetism, the interplay between spin interactions and lattice geometry crafts a fascinating landscape of ground states and excitations (e.g., see Refs. [1–3]). A central subject for this exploration is the XXZ Heisenberg model [4], a cornerstone that has deeply enriched our comprehension of anisotropic magnetic systems [5,6]. The model, celebrated for its versatility in representing real materials, allows for the examination of quantum fluctuations—the quintessential quantum mechanical effect that destabilizes classical magnetic order, paving the way for the emergence of novel quantum phases such as spin liquids [7,8].

This paper focuses on comparing the manifestations of quantum fluctuations within the $S = 1/2$ and $S = 1$ XXZ models on two fundamentally distinct lattice structures: the square and the honeycomb. These lattices, emblematic of different coordination environments and geometric constraints, provide a compelling backdrop against which the interplay of spin magnitude and lattice topology can be meticulously dissected. The square lattice, with its direct links to high-temperature superconductivity [9] and magnetic order [3] in solid-state compounds, and the honeycomb lattice, notable for hosting exotic phenomena such as the quantum spin Hall effect [10] and potential quantum spin liquid states [8], are ideal platforms for this comparative study.

Numerical simulations of such systems often pose significant challenges. When instantiated on a finite-size lattice, the total degrees of freedom exponentially increase with lattice size. This constraint on the geometry and size of the cluster becomes particularly notable for systems in more than two dimensions. Consequently, an extrapolation of physical quantity to an infinite system size is imperative to ascertain the bulk value. However, the execution of such finite-size scaling is usually fraught with challenges due to the presence of multiple scaling dimensions, such as the x and y directions in a two-dimensional (2D) case. In our previous studies [11,12], we introduced an efficient numerical method for determining the local order parameter in 2D systems through the use of spiral boundary conditions (SBCs). This method provides a promising approach to address the challenges associated with finite-size scaling in numerical simulations.

Applying SBCs allows for the exact projection of lattice models, even those extending beyond 2D, onto 1D periodic chains that maintain translational symmetry. Within this projected 1D chain, each lattice site is denoted by a single coordinate, contrary to the dual coordinates used in the original 2D cluster. This simplification means that only one finite-size scaling analysis along the chain direction is necessary to ascertain a physical quantity in the thermodynamic limit. We have demonstrated the capability of precisely determining the magnitude of staggered magnetization for the XXZ Heisenberg model on a square lattice ranging from $S = 1/2$

to 6 [12]. Here we consider the extension of this technique to studies of the honeycomb-lattice model and further demonstrate the systematic calculation of excitation energy in the bulk limit.

In this paper, we investigate the $S = 1/2$ and $S = 1$ XXZ Heisenberg models on square and honeycomb lattices employing the density-matrix renormalization group (DMRG) method. We delve into the evolution of staggered magnetization and the accompanying spin gap with easy-axis anisotropy. It is shown that by applying SBCs to both lattice types, a finite-size scaling analysis towards the thermodynamic limit can be effortlessly conducted for the studied physical quantities. The efficacy of our approach is corroborated by comparing our findings with pre-existing numerical and analytical results. Our analysis reveals that for most cases, the staggered magnetization and spin gap within the easy-axis Néel phase can be approximately accounted for by series expansions (SEs) of the 10th to 12th order in terms of $1/\Delta$. However, for the $S = 1/2$ honeycomb lattice, the results significantly deviate from those of the 10th-order SE across a broad range near the isotropic Heisenberg limit due to strong quantum fluctuations. Furthermore, for all models that are considered, we obtain results that are numerically consistent with the singular behavior of the spin gap near the isotropic Heisenberg limit as predicted by spin-wave theory (SWT). Also, we find a marked reduction in quantum fluctuations transitioning from $S = 1/2$ to $S = 1$ across all physical quantities that are assessed.

The paper is structured as follows: Sec. II provides a detailed description of our spin model. In Sec. III, we elucidate the method of mapping 2D models to 1D using SBCs, along with the procedures for calculating physical quantities via the DMRG technique. Section IV presents our numerical findings, examining the influence of lattice type, XXZ anisotropy magnitude, and spin size on the stability of staggered magnetization and the magnitude of the spin gap. Additionally, we incorporate a discussion on the specific behavior of the spin gap for the $S = 1/2$ honeycomb-lattice case. Finally, in Sec. V, we conclude the paper with a summary and further insights into the observed phenomena.

II. MODEL

The Hamiltonian of the XXZ Heisenberg model is represented as follows:

$$\mathcal{H} = \sum_{\langle ij \rangle} \left(S_i^x S_j^x + S_i^y S_j^y + \Delta S_i^z S_j^z \right), \tag{1}$$

where S_i^γ $(\gamma = x, y, z)$ are the spin-S operators, Δ is the anisotropy parameter, and the sum $\langle ij \rangle$ runs over all nearest-neighbor pairs. In this context, we consider two types of lattice structures: the square lattice and the honeycomb lattice. The XXZ models associated with these lattices have been significantly examined thus far.

There are three phases depending on Δ [13–17]: (i) For $\Delta > 1$ easy-axis Néel phase with antiferromagnetic (AFM) spin alignment along the z direction, (ii) for $-1 < \Delta < 1$ easy-plane Néel (XY) phase with AFM spin alignment along some arbitrary direction in the xy plane, and (iii) for $\Delta < -1$ ferromagnetic (FM) phase with fully polarized spins along the z direction. The phase transitions at $\Delta = \pm 1$ are both first order. For $\Delta = -1$, this model can be exactly solved: the Néel and FM states are degenerate at the ground state where the energies are $E_0 = -2NS^2$ and $E_0 = -(3/2)NS^2$ for square- and honeycomb-lattice models. The exact wave functions at $\Delta = -1$ were given in Ref. [12].

In regards to the square-lattice model, it has been numerically confirmed that for $S = 1/2$ [12,18], Néel long-range order (LRO) always exists for $\Delta > -1$. On the other hand, for the honeycomb-lattice model, due to fewer bonds between adjacent sites compared to the square lattice, quantum fluctuations are larger and there is not yet a complete consensus on which S and Δ regions stabilize Néel LRO [19,20].

III. METHOD

A. Spiral boundary conditions

Applying the DMRG method to 2D systems introduces significant challenges, primarily due to two factors. First, the entanglement entropy, which quantifies the quantum correlations within different parts of the system, follows an "area law." This law indicates that entanglement entropy scales with the boundary area of a region, complicating the simulation of large systems. Second, the DMRG's sweeping process, which optimizes quantum states site by site in a linear fashion in 1D systems, encounters difficulties in the more complex geometries of 2D systems. This complexity can lead to inaccuracies because a straightforward sweeping mechanism is harder to implement across 2D lattices.

To address these challenges, careful management of boundary conditions is essential for accurate DMRG simulations. Traditional approaches often employ cylinder or torus configurations for 2D systems. Yet, these configurations can create short bond loops and impose an unnatural periodicity on the wave function, leading to inaccuracies such as an unexpected plaquette constraint on particles or spins. An inappropriate choice of boundary conditions might also skew the energy states observed in finite clusters away from those relevant in the thermodynamic limit, instead of systematic errors due to the finite-size effects.

A promising alternative that circumvents these limitations involves the implementation of SBCs [11,21]. SBCs enables the exact projection of lattice models, including those extending beyond two dimensions, onto 1D periodic chains that preserve translational symmetry. This projection effectively transforms a 2D $L \times L$ cluster into a 1D chain, maintaining nearest-neighbor and $(L-1)$th-neighbor bonds for square lattices, and nearest- and $(2L-1)$th-neighbor bonds for honeycomb lattices, as depicted in Figs. 1(a) and 1(b). This innovative approach prevents the emergence of artificial short bond loops and ensures an even distribution of quantum entanglement across the chain, leveraging translational symmetry.

Notably, SBCs minimize the distance of the longest bonds, denoted as d, to $L-1$ for square and $2L-1$ for honeycomb lattices, optimizing conditions for DMRG calculations. In contrast, conventional periodic boundary conditions would increase d to $2L$ and $4L-2$, respectively, posing challenges for DMRG analysis.

Furthermore, SBCs provide a significant benefit for finite-size scaling analysis. By projecting the original 2D lattice onto a 1D chain, SBCs enable the indexing of each lattice

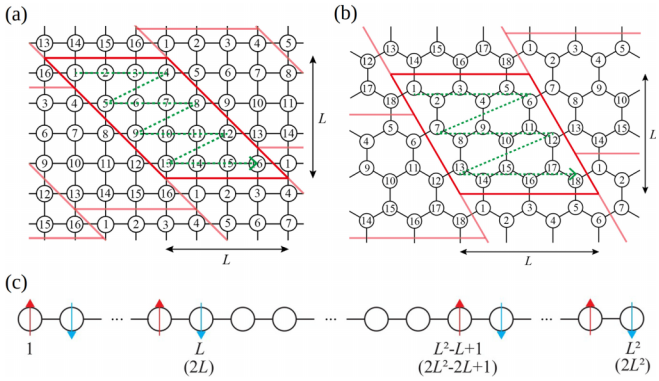

FIG. 1. (a) 2D square-lattice 4×4 cluster and (b) 2D honeycomb-lattice 3×3 cluster. The regions outlined by red lines represent the original clusters. Through the application of SBCs, the 2D clusters are projected onto 1D periodic chains, where the sites are aligned along the green lines. (c) Schematic depiction of the 1D open chain utilized for our DMRG calculations, focusing on staggered spin moment $m_\alpha^z(S, \Delta)$ and spin gap $\varepsilon_\alpha(S, \Delta)$. In the square lattice, pinning is applied to L sites at each end, while in the honeycomb lattice, pinning is applied to $2L$ sites. Upward and downward arrows signify pinned spins with $S^z = S$ and $S^z = -S$, respectively.

site with a singular coordinate, rather than the dual-coordinate system inherent to 2D clusters. This transition to a single-coordinate framework simplifies the analytical process to a unidimensional scale. It facilitates a more direct method for extrapolating physical quantities to the thermodynamic limit, enhancing the accuracy and efficiency of our simulations.

B. Density-matrix renormalization group

The investigation of the ground state of the 1D chain, transformed via SBCs, is conducted using the DMRG method [22]. For this purpose, we implement open boundary conditions on the 1D chain, a choice that significantly enhances the precision of our DMRG calculations. Our study encompasses open chains with lengths up to $N = L^2 = 196$ sites for the square lattice and up to $N = 2L^2 = 162$ sites for the honeycomb lattice. To ensure the robustness of our calculations, we retain up to $m = 8000$ density-matrix eigenstates, with all calculated values subsequently extrapolated to the limit of $m \to \infty$. The maximum discarded weight that is observed is of the order of 10^{-6}.

Furthermore, we intentionally break the spin-rotation symmetry by employing a spin pinning technique. This approach effectively lifts the degeneracy of the ground state, thereby efficiently reducing the dimensionality of the Hilbert space required for our calculations. As a result, even for computations of 2D systems, the discarded weight remains minimal, enhancing the accuracy and feasibility of our analysis.

C. Physical quantities

1. Staggered magnetization

We examine the Néel state for $\Delta \geqslant 1$, where the magnitude of staggered magnetization serves as the order parameter in both square and honeycomb lattice XXZ models. In the original 2D clusters, Néel order characterized by $\boldsymbol{k} = (\pi, \pi)$ is transformed into a magnetic order with $k = \pi$ along the projected 1D chain through our implementation of SBCs. For the analysis, we utilize open chains and determine the magnitude of staggered magnetization by measuring half the amplitude of the magnetization oscillation of $\langle S_i^z \rangle$ from the system edges. Given the condition $\Delta \geqslant 1$, it is sufficient to focus on the z component of the spin moment.

To establish such an open chain configuration, we sever L $(L + 1)$ bonds between adjacent sites on the projected 1D periodic chain for square (honeycomb) lattices, as described in recent works [12,23]. We specifically examine the local moments of the two central spins, $\langle S_{N/2}^z \rangle$ and $\langle S_{N/2+1}^z \rangle$, employing spin pinning near the system edges, such as setting $\langle S_i^z \rangle = (-1)^{i-1} S$ at sites $i = 1, \ldots, L$ and $i = L^2 - (L - 1), \ldots, L^2$ for the square lattice, and at sites $i = 1, \ldots, 2L$ and $i = 2L^2 - (2L - 1), \ldots, 2L^2$ for honeycomb lattice.

While pinning is typically positioned at the system edges, i.e., at $i = 1$, $i = N$, the last $L - 1$ $(2L - 1)$ sites at both ends of the projected 1D chain corresponding to a square (honeycomb) lattice are left without their original bonds, necessitating the placement of pinnings at these outer sites to accurately estimate staggered magnetization [see Fig. 1(c)]. Therefore, we define the magnitude of staggered magnetization for a given spin S and XXZ anisotropy Δ as

$$m_\alpha^z(S, \Delta) = \lim_{N \to \infty} \left| \langle S_{N/2}^z \rangle - \langle S_{N/2+1}^z \rangle \right| / 2. \tag{2}$$

Examples of local spin moment profiles, $\langle S_i^z \rangle$, for the $S^z = 0$ sector at $\Delta = 1$ are depicted in the top panels of Fig. 2. Here, the parameter α adopts the value "sq" for square lattices and "hon" for honeycomb lattices. In both square and honeycomb lattices, the oscillation of $\langle S_i^z \rangle$ smoothly decays towards the center of the system, validating the approach of defining the Néel order parameter via the local moments of the two central spins, $\langle S_{N/2}^z \rangle$ and $\langle S_{N/2+1}^z \rangle$.

2. Spin gap

The spin gap offers insight into phenomena such as quantum fluctuations and the stability of the Néel state. It also provides us with an understanding of how classical behavior emerges from quantum systems. The spin gap (singlet-triplet gap) for given S and Δ is defined as follows:

$$\varepsilon_\alpha(S, \Delta) = \lim_{N \to \infty} [E_0(N, 1) - E_0(N, 0)], \tag{3}$$

where $E_0(N, S^z)$ is the total ground-state energy of the system with N sites and the z component of the total spin, S^z. Here, the parameter α adopts the value "sq" for square lattices and "hon" for honeycomb lattices.

To verify the validity of our spin gap calculations under the imposed pinning distribution, we examine the spatial distribution of increased magnetization as the spin sector transitions from $S^z = 0$ to $S^z = 1$. The spatial distribution of the increased magnetization is visualized by observing the variance in $\langle S_i^z \rangle$ between the $S^z = 0$ and $S^z = 1$ sectors, denoted as $\delta \langle S_i^z \rangle$. We plot the profile of this distribution for $\Delta = 1$ in the bottom panels of Fig. 2. In both square and honeycomb lattices, it is observed that the presence probability of the increased magnetization is maximized near the center of the system, with minimal presence near the edges. This observation confirms that the spin gap in the bulk limit can be

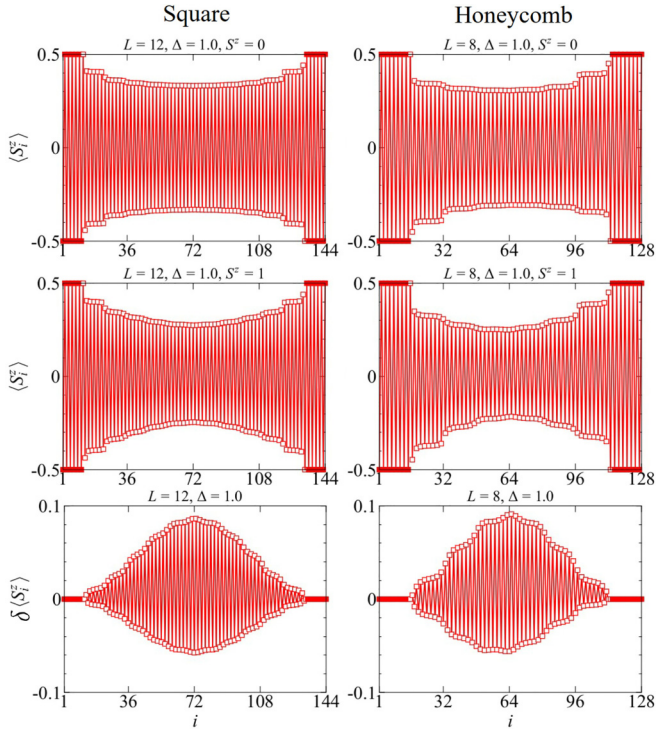

FIG. 2. Comparative profiles of the local spin moment for 12×12 square (left panels) and 8×8 honeycomb (right panels) lattices at spin-isotropic case $\Delta = 1$. The profiles depict $\langle S_i^z \rangle$, the expectation value of the z component of spin at site i, for two distinct total spin sectors: $S^z = 0$ (top row) and $S^z = 1$ (middle row). The bottom row illustrates the differential profiles, showing the variance in $\langle S_i^z \rangle$ between the $S^z = 0$ and $S^z = 1$ sectors.

correctly estimated using Eq. (3). We note that the distribution of $\langle S_i^z \rangle$ for the $S^z = 1$ sector and $\delta \langle S_i^z \rangle$ are asymmetric because the rotational symmetry as well as the mirror symmetry of the system is broken.

IV. RESULTS

A. Staggered magnetization

We start by looking at what we found about staggered magnetization. This measure adeptly quantifies the AFM alignment of magnetic moments throughout the lattice, offering profound insights into the stability and resilience of the Néel state against external perturbations. Our investigation spans two lattice configurations, i.e., square and honeycomb structures, and encompasses systems with spin magnitudes of $S = 1/2$ and $S = 1$. The primary objective of this analysis is to delineate the degree to which staggered magnetization is influenced by the lattice geometry and spin values.

1. Square lattice

In our preceding study [12], the magnitude of staggered magnetization for the $S = 1/2$ and $S = 1$ square-lattice XXZ Heisenberg models was quantified as a function of Δ. Here we revisit these results to consider the extent of quantum fluctuations in the Néel state at $\Delta \geqslant 1$. They are plotted in Fig. 3. For any S, the quantum fluctuations are maximized at

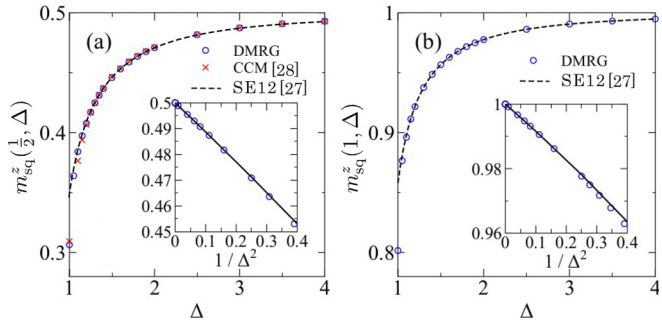

FIG. 3. Extrapolated values of $m_{sq}^z(S, \Delta)$ to the thermodynamic limit as a function of Δ for the (a) $S = 1/2$ and (b) $S = 1$ square-lattice XXZ models. Dashed lines represent the results from the SE up to the 12th order $1/\Delta$ [24–26]. Red crosses denote the results obtained via the CCM [27] for the $S = 1/2$ case. Insets: $m_{sq}^z(S, \Delta)$ vs $1/\Delta^2$ in the large-Δ region, with solid lines indicating the SE results up to the sixth order of $1/\Delta$.

$\Delta = 1$, correspondingly minimizing the staggered magnetization magnitude. The values of $m_{sq}^z(\frac{1}{2}, 1.0)$ and $m_{sq}^z(1, 1.0)$ estimated by various numerical methods are summarized in Table I. The differences in performance between our SBC method and previous DMRG studies is discussed in Appendix A. For $S = 1/2$, these values approximate 60% of the classical one, $m_{sq}^z(\frac{1}{2}, \infty) = 0.5$, while for $S = 1$, the staggered magnetization rises to about 80% of its classical counterpart, $m_z^{st}(1, \infty) = 1$. These results underscore the substantial suppression of quantum fluctuations with an increase in S. In fact, an expansion in terms of $1/S$ yields $m_{sq}^z(S, 1.0) = 1 - 0.196\,601\,9S^{-1} + 0.000\,87S^{-3} + O(S^{-4})$ [28–30]. Since the coefficients of higher-order terms than $1/S$ are very small, a rapid convergence to the classical (or Ising) limit $m_{sq}^z(S, 1.0)/S \to 1$ with increasing S is naively expected. This trend has received numerical validation [12].

To explore the evolution of quantum fluctuations with Δ, we compare our DMRG results to SE analyses. The deviation from the fixed-order SE results quantifies the extent of quantum fluctuations. The SE results are plotted as dotted lines in Fig. 3. At $\Delta = 1$, our DMRG analysis yields $m_{sq}^z(\frac{1}{2}, 1.0) = 0.3065$ and $m_{sq}^z(1, 1.0) = 0.8017$, whereas SE up to the 12th order (SE12) offers $m_{sq}^z(\frac{1}{2}, 1.0) = 0.3462$ and $m_{sq}^z(1, 1.0) = 0.8579$. Despite incorporating terms up to the 12th order, a discrep-

TABLE I. Magnitude of staggered magnetization for the $S = 1/2$ and $S = 1$ square-lattice Heisenberg models at the isotropic point ($\Delta = 1$), estimated using various numerical methods; DMRG, coupled cluster method (CCM), quantum Monte Carlo (QMC), and infinite projected entangled-pair states (iPEPS).

Method	$m_{sq}^z(\frac{1}{2}, 1.0)$	Refs.	Method	$m_{sq}^z(1, 1.0)$	Refs.
DMRG	0.3065	[12]	DMRG	0.8017	[12]
DMRG	0.3067	[31]	iPEPS	0.802	[32]
CCM	0.3093	[27]	SE	0.8039(4)	[26]
QMC	0.30743	[33]			
SE	0.307(1)	[26]			

ancy remains due to unaccounted quantum fluctuations, with a deviation of approximately 7.9% for $S = 1/2$ and 5.6% for $S = 1$. However, a slight increase in Δ to 1.05 yields $m^z_{\rm sq}(\frac{1}{2}, 1.05) = 0.3640$ (DMRG) and $m^z_{\rm sq}(\frac{1}{2}, 1.05) = 0.3678$ (SE12) for $S = 1/2$, and $m^z_{\rm sq}(1, 1.05) = 0.8767$ (DMRG) and $m^z_{\rm sq}(1, 1.05) = 0.8811$ (SE12) for $S = 1$, significantly reducing deviations to 0.76% and 0.44%, respectively. This suggests a pronounced reduction in quantum fluctuations attributable to XXZ anisotropy. In the $\Delta = \infty$ limit, SE approaches exactness, nullifying quantum fluctuations. To demonstrate the accuracy of our DMRG analyses, a comparison of our DMRG results with SE ones in the $\Delta = \infty$ limit is provided in Appendix B.

Additionally, in contrast to the singular behavior near $\Delta = 1$ predicted by SWT, which posits that $m^z_{\rm sq}(\frac{1}{2}, \Delta) = \sum_{n=0}^{\infty} m_n(\Delta - 1)^{n/2}$ [14,26,34], our observations reveal that $m^z_{\rm sq}(\frac{1}{2}, \Delta)$ is almost linearly proportional to $\Delta - 1$ within the range $1 \leqslant \Delta \lesssim 1.01$. This behavior aligns with results from the CCM [27]. However, we further ascertain that except in the immediate vicinity of $\Delta = 1$, the staggered magnetization for the square-lattice XXZ Heisenberg model at $\Delta \gtrsim 1$ can be approximately and quantitatively captured by SE, provided the expansion includes up to the 12th order of $1/\Delta$.

2. *Honeycomb lattice*

In exploring the honeycomb-lattice XXZ model, we note that each site is connected to three neighboring sites, a contrast to the four neighbors in the square-lattice model. This difference leads us to hypothesize that the Néel state in the honeycomb-lattice model might exhibit less stability compared to its counterpart in the square model due to the potential for increased quantum fluctuations. To investigate this, we delve into the dependence of staggered magnetization on the anisotropy parameter Δ for both $S = 1/2$ and $S = 1$ within the honeycomb lattice, drawing comparisons with our previous findings for the square-lattice model.

In Figs. 4(a) and 4(b), we perform finite-size scaling analyses for $m^z_{\rm hon}(\frac{1}{2}, \Delta)$ and $m^z_{\rm hon}(1, \Delta)$ over various values of Δ. Broadly, this scaling examines the decay of magnetization oscillations with distance from a spin pinned at the system edge. Given that the Néel state features a staggered (commensurate) arrangement of spins in our projected 1D chain, we anticipate a smooth decay of the magnetization oscillations with distance. This has been verified in Sec. III C 1. Consequently, $m^z_{\rm hon}(\frac{1}{2}, \Delta)$ and $m^z_{\rm hon}(1, \Delta)$ extrapolate smoothly to the thermodynamic limit as functions of inverse system size. Furthermore, the observation that convergence with respect to size occurs more rapidly as Δ increases reflects the diminishing quantum fluctuations. Unless otherwise specified, the finite-size scaling in this paper is performed using least-squares fitting with the fitting function $f(L) = a + bL^{-2} + cL^{-3}$. For all scaling analyses, the fraction of variance that is unexplained is estimated to be $1 - R^2 < 0.001$, where R^2 is the coefficient of determination.

The extrapolated values of $m^z_{\rm hon}(\frac{1}{2}, \Delta)$ and $m^z_{\rm hon}(1, \Delta)$ are plotted as a function of Δ in Figs. 4(c) and 4(d), respectively. In the case where the quantum fluctuations are largest at $\Delta = 1$, we obtain $m^z_{\rm hon}(\frac{1}{2}, 1.0) = 0.2764$ for $S = 1/2$ and $m^z_{\rm hon}(1, 1.0) = 0.7646$ for $S = 1$. These values are in close agreement with various numerical methods from previous studies. The values of $m^z_{\rm hon}(\frac{1}{2}, 1.0)$ and $m^z_{\rm hon}(1, 1.0)$ estimated by various numerical methods are summarized in Table II. Our estimations are ∼55% and ∼76% of their respective classical values, only slightly smaller despite the greater quantum fluctuations compared to the square-lattice case. On the other hand, the SE analyses up to the 12th order of $1/\Delta$ lead to $m^z_{\rm hon}(\frac{1}{2}, 1) = 0.3409$ and $m^z_{\rm hon}(1, 1) = 0.8139$ for $S = 1/2$ and $S = 1$, respectively. These values, when compared with those obtained from our DMRG simulations, exhibit discrepancies of 6.5% for $S = 1/2$ and 4.9% for $S = 1$. Interestingly, these deviations are rather smaller than those observed for the square lattice, where the discrepancies are notably lower

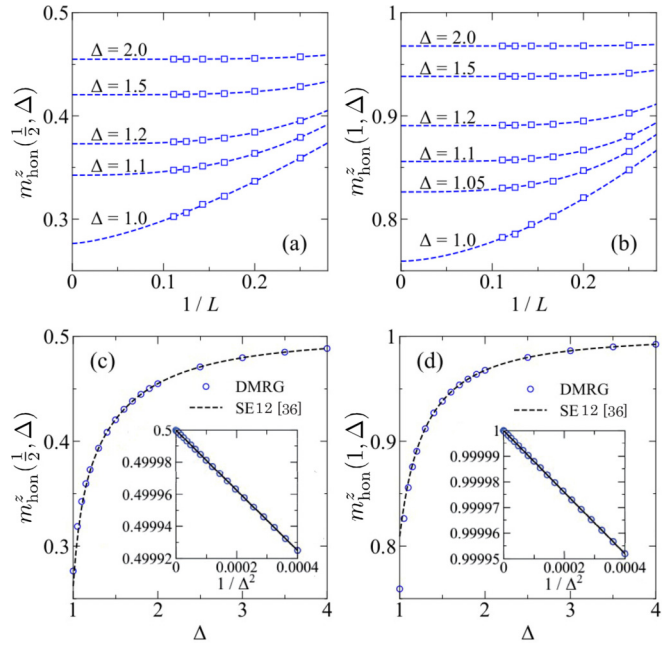

FIG. 4. Magnitude of staggered magnetization for the $S = 1/2$ and $S = 1$ honeycomb-lattice XXZ models as a function of Δ. Finite-size scaling analyses of (a) $m^z_{\rm hon}(\frac{1}{2}, \Delta)$ and (b) $m^z_{\rm hon}(1, \Delta)$. Extrapolated values of (c) $m^z_{\rm hon}(\frac{1}{2}, \Delta)$ and (d) $m^z_{\rm hon}(1, \Delta)$ to the thermodynamic limit as a function of Δ. The dashed lines show the SE results up to the 12th order of $1/\Delta$ [35]. Insets: $m^z_{\rm hon}(S, \Delta)$ vs $1/\Delta^2$ in the large-Δ region. Solid lines represent the SE results up to the 6th order of $1/\Delta$.

TABLE II. Magnitude of staggered magnetization for the $S = 1/2$ and $S = 1$ honeycomb-lattice Heisenberg models at the isotropic point ($\Delta = 1$), estimated using various numerical methods.

Method	$m^z_{\rm hon}(\frac{1}{2}, 1.0)$	Refs.	Method	$m^z_{\rm hon}(1, 1.0)$	Refs.
DMRG	0.2764	this study	DMRG	0.7646	this study
DMRG	0.2857	[36]	CCM	0.7412	[18]
DMRG	0.2720	[37]	SE	0.748(3)	[35]
DMRG	0.2611	[38]			
CCM	0.2730	[18]			
QMC	0.2677	[39]			
ED	0.262	[40]			
SE	0.266(9)	[35]			

at 7.9% for $S = 1/2$ and 5.6% for $S = 1$. Furthermore, the increase in magnetization when S changes from 1/2 to 1 is similar to that in the square lattice. This may be expected from the coefficients of the $1/S$ series expansion for the honeycomb lattice, $m^z_{\rm hon}(S, 1.0) = 1 - 0.258\,193/S + \cdots$ [14], which are close to those for the square lattice.

Let us then see the Δ dependence. As illustrated in Figs. 4(c) and 4(d), the magnetization rapidly approaches classical values with increasing Δ. It is also evident that apart from the immediate vicinity of $\Delta = 1$, the magnetization is well captured by the SE12 predictions. Indeed, a slight increase in Δ from 1 to 1.05 yields $m^z_{\rm hon}(\frac{1}{2}, 1.05) = 0.3188$ (DMRG) versus $m^z_{\rm hon}(\frac{1}{2}, 1.05) = 0.3478$ (SE12) for $S = 1/2$, and $m^z_{\rm hon}(1, 1.05) = 0.8242$ (DMRG) versus $m^z_{\rm hon}(1, 1.05) = 0.8427$ (SE12) for $S = 1$. The discrepancies between the DMRG and SE12 values significantly decrease from 6.5% and 4.9% at $\Delta = 1$ to 2.9% and 1.9% at $\Delta = 1.05$ for $S = 1/2$ and $S = 1$, respectively. Nevertheless, the quantum fluctuations remain comparatively large and thus the reduction is not as dramatic as in the case of the square lattice (see Sec. IV A 1). A comparison of our DMRG results with SE ones in the $\Delta = \infty$ limit is provided in Appendix B.

Thus, our examination of the honeycomb-lattice XXZ model reveals that akin to the case for a square lattice, staggered magnetization can be reasonably approximated by SE12 for $\Delta > 1$.

B. Spin gap

Next, we delve into the investigation of the spin gap, which serves as an indicator of the stability of Néel LRO when spin-rotation symmetry about the z axis is explicitly broken by staggered magnetization. This parameter is essential for understanding the energy required to excite the system from its Néel ground state, a facet less explored compared to direct magnetization measurements. Employing methodologies analogous to those used in our magnetization studies, we extend our analysis to both square- and honeycomb-lattice configurations for $S = 1/2$ and $S = 1$ systems. Our aim is to elucidate the behavior of the spin gap across varying lattice geometries and spin magnitudes, offering insights into the intricacies associated with excitations from the Néel state.

1. Square lattice

Let us first examine the spin gap in the case of a square lattice. In Figs. 5(a) and 5(b), finite-size scaling analyses for $\varepsilon_{\rm sq}(\frac{1}{2}, \Delta)$ and $\varepsilon_{\rm sq}(1, \Delta)$ are shown across various values of Δ. Our scaling analysis reveals that a smooth extrapolation of the spin gap often suggests that the scaling function resembles the contour of a magnon band near the Fermi level. For both spin magnitudes at $\Delta = 1$, the spin-gap data closely align with a linear fit, extrapolating towards zero in the thermodynamic limit, albeit with minor numerical uncertainties inherent to the extrapolation process. This linear fit aligns with expectations for gapless systems where the linear magnon band structure near the Fermi points dominates. The actual values of the extrapolated spin gap are $\varepsilon_{\rm sq}(\frac{1}{2}, 1) = -0.001\,700\,06$ and $\varepsilon_{\rm sq}(1, 1) = 0.006\,843\,18$. This hints at a Néel LRO that despite being stable, exhibits a spin gap of zero due to the arbitrary direction of symmetry breaking. Moreover, at slightly

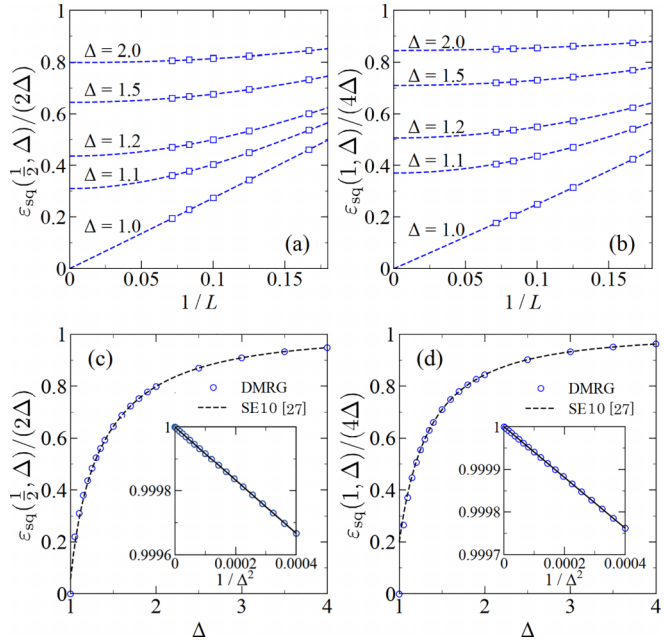

FIG. 5. Spin gap for the $S = 1/2$ and $S = 1$ square-lattice XXZ models as a function of Δ. Finite-size scaling analyses of (a) $\varepsilon_{\rm sq}(\frac{1}{2}, \Delta)$ and (b) $\varepsilon_{\rm sq}(1, \Delta)$. Extrapolated values of (c) $\varepsilon_{\rm sq}(\frac{1}{2}, \Delta)$ and (d) $\varepsilon_{\rm sq}(1, \Delta)$ to the thermodynamic limit as a function of Δ. The dashed lines show the SE results up to the 10th order of $1/\Delta$ [26]. Insets: $\varepsilon_{\rm sq}(S, \Delta)$ in the large-Δ region. Solid lines represent the SE results up to the 6th order of $1/\Delta$.

increased values of Δ, namely, 1.1 and 1.2, the observed small gaps corroborate the quadratic dispersion expected near the Fermi points. As the gap widens, quantum fluctuations wane, leading to a narrower bandwidth and, thus, a diminished size dependence of the gap. Utilizing SBCs to transform the 2D lattice into an effective 1D system allows for the original 2D Fermi surface to be conceptualized as a "Fermi line," aiding in the smooth scaling of the gap.

Figures 5(c) and 5(d) display the extrapolated spin gaps $\varepsilon_{\rm sq}(\frac{1}{2}, \Delta)$ and $\varepsilon_{\rm sq}(1, \Delta)$, showcasing a trend similar to that of magnetization with increasing Δ, rapidly approaching the classical values $4\Delta S$. Excluding the region immediately around $\Delta = 1$, the behavior of the spin gap correlates well with SE predictions up to the 10th order in $1/\Delta$. A comparison of our DMRG results with SE ones in the $\Delta = \infty$ limit is provided in Appendix C.

Investigating the behavior of the spin gap near $\Delta = 1$, SWT anticipates a singularity, encapsulated by the following relation:

$$\frac{\varepsilon}{\Delta} = \eta_1(1 - \Delta^{-2})^{1/2} + \eta_2(1 - \Delta^{-2}) + \eta_1(1 - \Delta^{-2})^{3/2} + \cdots, \tag{4}$$

with constants $\eta_1 = 4S - 0.431\,436$ and $\eta_2 = 1.2732$ derived from SWT predictions [41]. To scrutinize this predicted behavior, we present DMRG results for the normalized spin gap, $\frac{\varepsilon}{\Delta}$, as a function of $1 - \Delta^{-2}$ around $\Delta = 1$ in Figs. 6(a) and 6(b). For both $S = 1/2$ and $S = 1$, we can reasonably fit our DMRG data by Eq. (4), yielding $\eta_1 = 1.363\,949\,87$, $\eta_2 = 0.066\,724\,577\,2$, $\eta_3 = 0.572\,388\,620$ for $S = 1/2$ and $\eta_1 =$

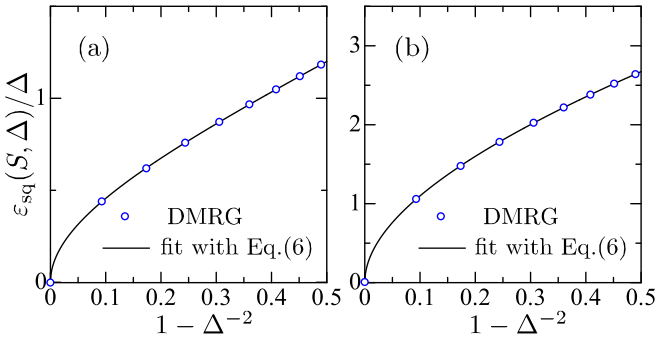

FIG. 6. Δ-normalized spin gap for the (a) $S = 1/2$ and (b) $S = 1$ square-lattice XXZ models as a function of $1 - \Delta^{-2}$. Circles denote DMRG results in the thermodynamic limit, while the solid line represents a fit using Eq. (4).

3.234 503 60, $\eta_2 = 0.754\,467\,400$, $\eta_3 = 0.022\,688\,166\,0$ for $S = 1$. These leading coefficients are close to the SWT prediction of $\eta_1 = 1.568\,564$ for $S = 1/2$ and $\eta_1 = 3.568\,564$ for $S = 1$, indicating an increase in η_1 with S, consistent with the fact that in the large-S limit, the gap jumps to $\varepsilon_{\rm sq}(S = \infty, \Delta = 1^+) = 4\Delta S$ as soon as XXZ anisotropy is introduced. Our numerical investigation thus substantiates the SWT-predicted singularity in the spin gap near $\Delta = 1$. Nonetheless, for $S = 1/2$, contrasting viewpoints emerge, such as those from CCM analyses, which suggest a near-linear relation, $\varepsilon \propto \Delta$, diverging from the expected singular behavior. This discrepancy could arise from our extrapolations to the thermodynamic limit, particularly near $\Delta = 1$, which are marginally higher than those deduced from CCM. As a reference, Table III compares the spin-gap values derived from DMRG and CCM for various Δ settings in the $S = 1/2$ case. A more in-depth examination will be imperative in future studies to resolve these discrepancies and fully delineate the characteristics of the spin gap near $\Delta = 1$.

2. *Honeycomb lattice*

Finally, we examine the spin gap for the honeycomb-lattice model. In Figs. 7(a) and 7(b), we conduct finite-size scaling analyses for $\varepsilon_{\rm hon}(\frac{1}{2}, \Delta)$ and $\varepsilon_{\rm hon}(1, \Delta)$ over various values of Δ. We see that smooth scaling is possible for all values of Δ,

TABLE III. Comparison of spin gaps as a function of Δ for the $S = 1/2$ square-lattice XXZ Heisenberg model obtained via DMRG and CCM calculations.

	$\varepsilon_{\rm sq}(\frac{1}{2}, \Delta)$			$\varepsilon_{\rm sq}(\frac{1}{2}, \Delta)$	
Δ	DMRG	CCM	Δ	DMRG	CCM
1.00	−0.0017	−0.0086	1.60	2.1995	2.2279
1.10	0.6810	0.5601	1.70	2.4578	2.4921
1.15	0.8722	0.7811	1.80	2.7083	2.7465
1.20	1.0461	0.9805	1.90	2.9535	2.9934
1.25	1.2088	1.1646	2.00	3.1942	3.2344
1.30	1.3627	1.3371	2.50	4.3496	4.3828
1.35	1.5118	1.5004	3.00	5.4546	5.4790
1.40	1.6560	1.6563	3.50	6.5306	6.5481
1.50	1.9334	1.9509	4.00	7.5880	7.6008

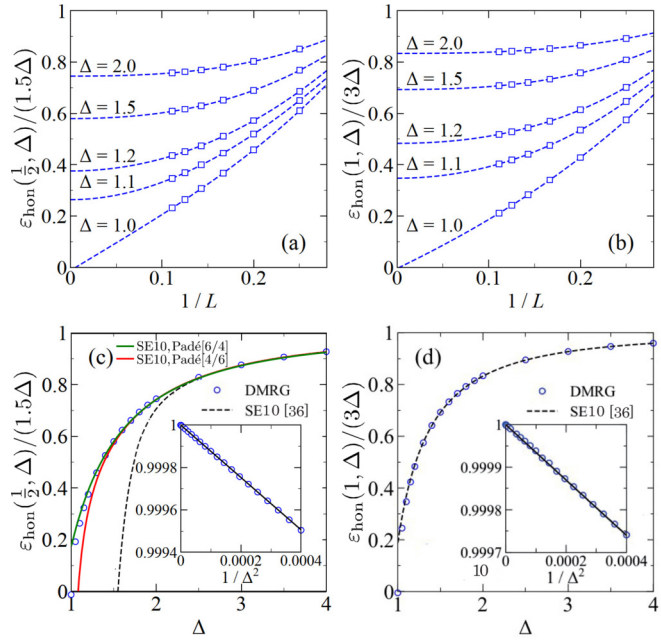

FIG. 7. Spin gap for the $S = 1/2$ and $S = 1$ honeycomb-lattice XXZ models as a function of Δ. Finite-size scaling analyses of (a) $\varepsilon_{\rm hon}(\frac{1}{2}, \Delta)$ and (b) $\varepsilon_{\rm hon}(1, \Delta)$. Extrapolated values of (c) $\varepsilon_{\rm hon}(\frac{1}{2}, \Delta)$ and (d) $\varepsilon_{\rm hon}(1, \Delta)$ to the thermodynamic limit as a function of Δ. The dashed lines show the SE results up to the 10th order of $1/\Delta$ [35] and the solid lines show the the Padé approximant applied to the SE10 results. Insets: $\varepsilon_{\rm sq}(S, \Delta)$ in the large-Δ region. Solid lines represent the SE results up to the 6th order of $1/\Delta$.

similar to the case of the square lattice. Consistently, at $\Delta = 1$, the scaling function is almost linear, approaching to nearly zero as $1/L$ decreases; while for $\Delta > 1$, a quadratic behavior indicative of gap opening is observed. The actual extrapolated values are $\varepsilon_{\rm hon}(\frac{1}{2}, 1) = -0.019\,166\,48$ and $\varepsilon_{\rm hon}(1, 1) = -0.014\,476\,16$, indicating slight but larger deviations from zero than those observed in the square-lattice case. The square lattice, having one site per structural unit cell, allowed calculations up to $L = 14$, whereas the honeycomb lattice, with two sites per structural unit cell, limits computations to $L = 9$ for a comparable computational cost, potentially leading to relatively larger scaling errors towards the thermodynamic limit in the honeycomb-lattice case.

The extrapolated values of $\varepsilon_{\rm hon}(\frac{1}{2}, \Delta)$ and $\varepsilon_{\rm sq}(1, \Delta)$ are plotted as a function of Δ in Figs. 7(c) and 7(d), showing a behavior broadly similar to the magnetization versus Δ relationship. Interestingly, the saturation towards the classical value $3\Delta S$ seems to be more gradual than observed in the square-lattice case, due to the heightened quantum fluctuations.

A notable finding is that SE analyses up to the 10th order in $1/\Delta$ are almost inapplicable in the region $\Delta \lesssim 2$ for $S = 1/2$. Due to the large coefficients of higher-order terms, adding each successive term causes significant oscillations near $\Delta = 1$, making approximation solely by SE very challenging in this vicinity (see Appendix D). Nevertheless, the SE10 curve is significantly improved by applying the Padé approximant. However, the value of $\varepsilon_{\rm hon}(\frac{1}{2}, \Delta)$ remains not very close to 0 at $\Delta = 1$: −1.1318 from the Padé approximant of order [4/6]

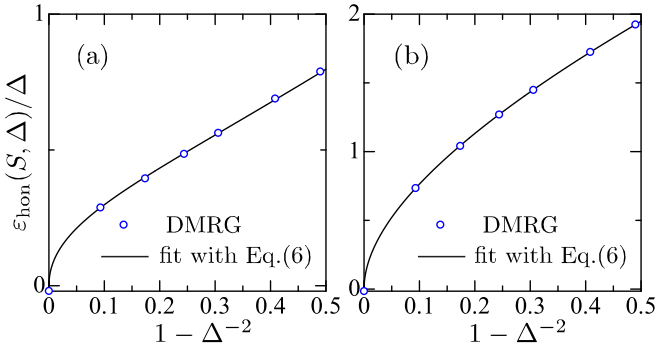

FIG. 8. Δ-normalized spin gap for the (a) $S = 1/2$ and (b) $S = 1$ honeycomb-lattice XXZ models as a function of $1 - \Delta^{-2}$. Circles denote DMRG results in the thermodynamic limit, while the solid line represents a fit using Eq. (4).

and 0.2683 from that of order [6/4]. These findings emphasize the critical influence of quantum fluctuations on the spin excitation in its Néel state. Conversely, for $S = 1$, the SE results up to the 10th order in $1/\Delta$ can reasonably describe the general gap behavior, except in the immediate vicinity of $\Delta = 1$. The Padé approximant provides $\varepsilon_{\rm hon}(1, \Delta) = 0.5571$ and 0.4284 from its orders [4/6] and [6/4], respectively. Furthermore, a comparison of our DMRG results with SE ones in the $\Delta = \infty$ limit is provided in Appendix C.

In alignment with observations for the square lattice, SWT also forecasts singular behavior near $\Delta = 1$ for the honeycomb lattice. The asymptotic form of this behavior is encapsulated by Eq. (4), with SWT providing the coefficients as $\eta_1 = 3S - 0.423\,239$ and $\eta_2 = 1.2405$ [14]. To verify if our DMRG data align with these predictions, we analyze the normalized spin gap, $\frac{\varepsilon}{\Delta}$, as a function of $1 - \Delta^{-2}$ approaching $\Delta = 1$, as depicted in Figs. 8(a) and 8(b).

Our fits to Eq. (4) for both $S = 1/2$ and $S = 1$ seem to be reasonable and yield $\eta_1 = 1.030\,931\,09$, $\eta_2 = -0.614\,589\,918$, $\eta_3 = 1.062\,001\,53$ for $S = 1/2$, and $\eta_1 = 2.129\,142\,13$, $\eta_2 = 0.923\,738\,066$, $\eta_3 = -0.055\,019\,266\,1$ for $S = 1$. These leading coefficients exhibit a notable correspondence with SWT-anticipated $\eta_1 = 1.076\,761$ for $S = 1/2$ and $\eta_1 = 2.576\,761$ for $S = 1$, underscoring our numerical validation of the predicted singularity in the spin gap as Δ approaches 1. Incidentally, the observation that η_1 for $S = 1$ is larger than that for $S = 1/2$ suggests a trend towards the discontinuity where the gap leaps to $\varepsilon_{\rm sq}(S = \infty, \Delta = 1^+) = 3\Delta S$ with the introduction of XXZ anisotropy in the limit of $S = \infty$.

V. SUMMARY AND DISCUSSION

We have achieved a comprehensive study of the $S = 1/2$ and $S = 1$ XXZ Heisenberg model on square and honeycomb lattices. By employing the DMRG method, we systematically analyzed the evolution of staggered magnetization and the associated spin gap across a wide range of easy-axis anisotropies. A key to enhancing DMRG performance was the implementation of SBCs, which enabled an exact mapping of the original 2D clusters onto a 1D chain. This technique significantly improved our ability to perform efficient finite-size scaling analysis, thereby facilitating the extrapolation of physical quantities to the thermodynamic limit with high accuracy. This methodological innovation opens new avenues for the study of quantum phenomena in complex lattice systems, providing a robust framework for exploring the effects of lattice geometry and spin interactions on magnetic order and excitations.

Given the difference in the number of adjacent sites—four for the square lattice versus three for the honeycomb lattice—it is reasonable to anticipate greater quantum fluctuations in the Néel phase for the honeycomb structure. This implies a potentially lower stability of the Néel LRO in the honeycomb lattice as compared to the square lattice. Contrary to what might be expected from the increased quantum fluctuations, we found that the magnitude of staggered magnetization in the honeycomb lattice is only marginally smaller than that in the square lattice. Furthermore, across all models that are investigated, the dependence of staggered magnetization on Δ, except very close to $\Delta = 1$, is well captured by SE up to the 12th order. The Δ dependence of the spin gap closely mirrors that of staggered magnetization, with most cases being approximately describable by SE up to the 10th order. However, for the $S = 1/2$ honeycomb lattice, significant deviations from the 10th-order SE predictions are observed near the isotropic Heisenberg limit, underscoring the pivotal role of quantum fluctuations on the spin gap in its Néel state. Moreover, for all models that are considered, our results align numerically with the singular behavior of the spin gap near the isotropic Heisenberg limit as predicted by SWT.

Finally, we delve into why the Δ dependence of the spin gap for the $S = 1/2$ honeycomb-lattice case largely deviates from the high-order SE results compared to other model cases, although its Δ dependence of staggered magnetization can be approximately explained by the SE analyses for most of the Δ range. To consider this issue, we calculate the ratio of the spin gap to the magnitude of magnetization, defined for the square and honeycomb lattices, respectively, as

$$r_{\rm sq}(S, \Delta) = \frac{\varepsilon_{\rm sq}(S, \Delta)}{4\Delta m^z_{\rm sq}(S, \Delta)}, \quad r_{\rm hon}(S, \Delta) = \frac{\varepsilon_{\rm hon}(S, \Delta)}{3\Delta m^z_{\rm hon}(S, \Delta)}. \tag{5}$$

This quantity can be an indicator of the stability of staggered magnetization in the z direction within the Néel LRO. In the isotropic case $\Delta = 1$, where quantum fluctuations are maximized, the ratio becomes 0, while in the classical limit $\Delta = \infty$, where quantum fluctuations are absent, it becomes 1. The ratios for all four models are plotted as a function of Δ in Fig. 9(a). As expected, the $r_{\rm hon}(\frac{1}{2}, \Delta)$ curve is apparently lower than the other three cases, implying a relatively unstable Néel LRO. In other words, the wave function contains more components with disordered spin configurations. This is consistent with the larger coefficients for higher-order terms in SE (see Appendix D). We also plot the differences between $r_{\rm hon}(\frac{1}{2}, \Delta)$ and the other three ratios in Fig. 9(b), revealing large deviations at $\Delta \approx 1$ to 2. This means that introducing XXZ anisotropy rapidly stabilizes the Néel LRO in the three models compared to the $S = 1/2$ honeycomb-lattice model. Interestingly, this quantity appears less dependent on the lat-

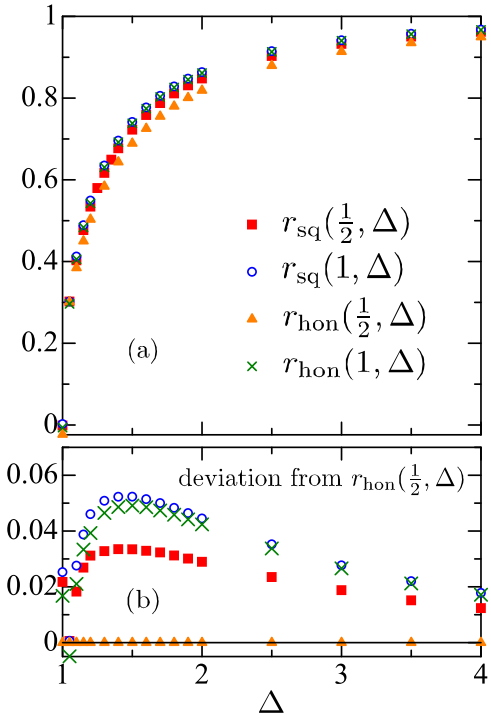

FIG. 9. (a) Ratio of the spin gap to the magnitude of magnetization, which is normalized to approach unity in the classical limit, as a function of Δ for the the $S = 1/2$ and $S = 1$ XXZ Heisenberg models on square and honeycomb lattices. (b) The values plotted in (a) subtracted by $r_{\rm hon}(\frac{1}{2}, \Delta)$.

tice geometry for $S = 1$. For reference, the data in Fig. 9 are shown in Appendix E.

Although we focus on the range of $\Delta \leqslant 1$ in this paper, a similar calculation for the magnitude of staggered magnetization is possible by applying a pinning field, e.g., along the x axis for the region of Δ between -1 and 1. However, calculating the spin gap becomes more challenging since Eq. (3) cannot be used due to the nonconservation of total S^z. It would be necessary to target the excitation energies or evaluate the dynamical response when a spin is flipped.

ACKNOWLEDGMENTS

We thank U. Nitzsche for technical support. This work was supported by Grants-in-Aid for Scientific Research from JSPS (Projects No. JP20H01849, No. JP20K03769, and No. JP21J20604). M.K. acknowledges support from the JSPS Research Fellowship for Young Scientists. M.N. acknowledges the research fellow position of the Institute of Industrial Science, The University of Tokyo. S.N. acknowledges support from SFB 1143 project A05 (Project ID No. 247310070) of the Deutsche Forschungsgemeinschaft.

APPENDIX A: COMPARISON OF STAGGERED MAGNETIZATION AT $\Delta = 1$ WITH PREVIOUS DMRG STUDIES

In this Appendix, we discuss the differences in performance between the SBC method used in this paper to determine the staggered magnetization at $\Delta = 1$ and the methods used in previous DMRG studies.

For the $S = 1/2$ square-lattice case, we estimated $m^z_{\rm sq}(\frac{1}{2}, 1.0) = 0.3065$, whereas Ref. [31] estimated 0.3067. In Ref. [31], a cylindrical cluster was used; importantly, the lattice is tilted by 45° to avoid the formation of plaquette singlets along the circumference. Additionally, similar to our approach, a staggered pinning field is applied to the open edges. This pinning significantly reduces the global quantum fluctuations in the system, thus improving the accuracy of the DMRG calculations. By enlarging the cluster to 14×12 while maintaining the aspect ratio of the cluster in the x and y directions, the thermodynamic limit value can be obtained with a single finite-size scaling analysis. Therefore, due to the comparable precision and computational cost, our results are very close to those obtained in Ref. [31]. The difference of 0.0002 is within the margin of error for size scaling.

For the $S = 1/2$ honeycomb-lattice case, there is some variation in the values of $m^z_{\rm hon}(\frac{1}{2}, 1.0)$ obtained from previous DMRG studies, including our result of 0.2764. Previous studies have reported values of 0.2857 [36], 0.2720 [37], and 0.2611 [38]. In Ref. [37], so-called XC cylinders were used. To minimize finite-size effects, lattices of size 8×8, 10×10, and 12×12 were employed, with the magnetization measured at the center of the cylinder, while applying a pinning field at both edges. This method is similar to ours, with comparable computational costs and an expectation of highly accurate staggered magnetization estimates. However, due to the limited data points (only three sizes), finite-size scaling was not performed, although the size dependence appears to be small.

In Refs. [36,38], different clusters were used; the former employed an open cluster and the latter used a so-called $ZCL - 2L$ cylinder, but the method for determining magnetization was the same. They obtained the thermodynamic limit value of $m^z_{\rm hon}(\frac{1}{2}, 1.0)^2$ via finite-size scaling of the static spin structure factor at the (π, π) mode and then took the square root to find $m^z_{\rm hon}(\frac{1}{2}, 1.0)$. Additionally, both studies used clusters without fields at the system edges, which may lead to higher computational costs for accurate DMRG calculations, potentially limiting the cluster size. As a result, finite-size scaling is not straightforward and the scaling error may be amplified when taking the square root. This reasoning may explain why our result is close to 0.2720 [37]. However, it should be noted that Refs. [36–38] were designed to investigate the magnetic properties of the $J_1 - J_2$ Heisenberg model on a honeycomb lattice and were not necessarily optimized for results at $J_2 = 0$.

APPENDIX B: COMPARISON OF STAGGERED MAGNETIZATION BETWEEN DMRG AND SE RESULTS IN THE $\Delta = \infty$ LIMIT

In the limit of $\Delta = \infty$, the SE analysis approaches exactness since quantum fluctuations disappear. To demonstrate the accuracy of our DMRG method, we compare our results with the SE ones for the staggered magnetization of the XXZ Heisenberg model in spin-1/2 and spin-1 systems on square and honeycomb lattices.

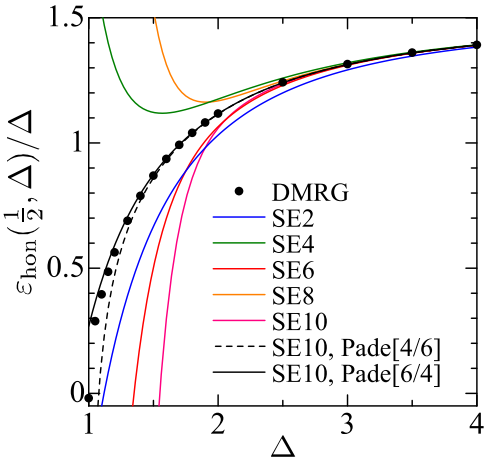

FIG. 10. Δ-normalized spin gap for the $S = 1/2$ honeycomb-lattice case obtained via DMRG and SE, plotted as a function of Δ. Here, the SE results incorporating terms up to the nth order are denoted as SEn. The Padé approximant applied to the SE10 results is also shown.

For the square lattice, utilizing SE up to the sixth order in $1/\Delta$, we express the staggered magnetization for $S = 1/2$ systems as $2m^z_{\rm sq}(\frac{1}{2},\Delta) = 1 + m_2/\Delta^2 + m_4/\Delta^4 + m_6/\Delta^6$. The coefficients are calculated to be $m_2 = -2/9 = -0.222\,222\ldots$, $m_4 = -8/255 = -0.035\,555\,5\ldots$, and $m_6 = -0.018\,942\,58$ for $S = 1/2$ [24,26,34,42,43]. In the case of $S = 1$ systems, staggered magnetization is similarly formulated as $m^z_{\rm sq}(1,\Delta) = 1 + m_2/\Delta^2 + m_4/\Delta^4 + m_6/\Delta^6$, with coefficients $m_2 = -4/49 = -0.081\,632\,653\ldots$, $m_4 = -0.026\,959\,099$, and $m_6 = -0.013\,699\,751\,5$ [25,26]. The magnitude of the lowest-order term, i.e., m_2, for $S = 1/2$ is approximately 2.7 times that for $S = 1$, implying a significant difference in quantum fluctuations between the two. Fitting our data for $0 \leqslant 1/\Delta \leqslant 0.05$, we obtain $m_2 = -0.222\,222\,225$, $m_4 = -0.035\,554\,273\,6$, and $m_6 = -0.018\,966\,381\,0$ for $S = 1/2$, and $m_2 = -0.081\,632\,653$, $m_4 = -0.026\,959\,397$, and $m_6 = -0.013\,867\,377$ for $S = 1$. These coefficients are in almost perfect agreement with the SE results.

For the honeycomb lattice, by employing expansions up to the fourth order in $1/\Delta$, the staggered magnetization for both spin-1/2 and $S = 1$ systems can be expressed as $m_z(S = 1/2) = 0.5 - m_2/\Delta^2 + m_4/\Delta^4 + o(1/\Delta^6)$. The coefficients are found to be $m_2 = -3/16 = -0.1975$, $m_4 = 31/768 = 0.040\,364\,583\,3\ldots$ for $S = 1/2$ and $m_2 = -3/25 = -0.12$, $m_4 = -17\,977/54\,000 = -0.332\,907\,4\ldots$ for $S = 1$ [35]. Fitting our data for $0 \leqslant 1/\Delta \leqslant 0.02$, we obtain $m_2 = -0.187\,499\,964$, $m_4 = 0.039\,452\,368\,2$ for $S = 1/2$ and $m_2 = -0.120\,000\,004$, $m_4 = -0.033\,243\,009\,9$ for $S = 1$. These values are in good agreement with those from SE.

APPENDIX C: COMPARISON OF SPIN GAP BETWEEN DMRG AND SE RESULTS IN THE $\Delta = \infty$ LIMIT

We conduct a similar analysis of the spin gap in the limit of $\Delta = \infty$ as we did for the staggered magnetization in Appendix B.

For the square lattice, the SE up to the second order in $1/\Delta$ formulates $\varepsilon_{\rm sq}(S,\Delta) = 2 + m_2/\Delta^2 + \mathcal{O}(1/\Delta^4)$, where m_2 equals $-5/3 = 1.666\,666\,6\cdots$ for $S = 1/2$ and $-50/21 = 2.380\,952\,3\cdots$ for $S = 1$. Our data fitting for $0 \leqslant 1/\Delta \leqslant 0.02$ yields $m_2 = -1.668\,031\,35$ for $S = 1/2$ and $m_2 = -2.379\,968\,04$ for $S = 1$, in close agreement with these SE coefficients, demonstrating the validity of our method.

For the honeycomb lattice, the SE up to the second order in $1/\Delta$ is expressed as $\varepsilon_{\rm hon}(S,\Delta) = 2 + m_2/\Delta^2 + \mathcal{O}(1/\Delta^4)$, where the coefficients are determined to be $m_2 = -15/8 = 1.875$ for $S = 1/2$ and $m_2 = -39/20 = 1.95$ for

TABLE IV. Extrapolated values of staggered magnetization, spin gap, and their ratio defined by Eq. (5) to the thermodynamic limit as a function of Δ for the $S = 1/2$ square-lattice XXZ Heisenberg model obtained by our DMRG calculations.

	$S = 1/2$			$S = 1$		
Δ	$\varepsilon_{\rm sq}(\frac{1}{2},\Delta)$	$m^z_{\rm sq}(\frac{1}{2},\Delta)$	$r_{\rm sq}(\frac{1}{2},\Delta)$	$\varepsilon_{\rm sq}(1,\Delta)$	$m^z_{\rm sq}(1,\Delta)$	$r_{\rm sq}(1,\Delta)$
1.00	−0.00170	0.30651	−0.00139	0.00684	0.80170	0.00213
1.05	0.46158	0.36402	0.30191	1.11193	0.87667	0.30199
1.10	0.68102	0.38422	0.40284	1.62512	0.89616	0.41214
1.15	0.87217	0.39752	0.47696	2.04938	0.91139	0.48883
1.20	1.04607	0.40789	0.53429	2.42961	0.92172	0.54915
1.30	1.36273	0.42488	0.61679	3.09541	0.93763	0.63487
1.40	1.65602	0.43681	0.67699	3.69616	0.94862	0.69578
1.50	1.93344	0.44593	0.72262	4.25626	0.95670	0.74149
1.60	2.19954	0.45312	0.75847	4.78831	0.96291	0.77699
1.70	2.45781	0.45891	0.78761	5.29980	0.96780	0.80532
1.80	2.70835	0.46366	0.81128	5.79559	0.97174	0.82836
1.90	2.95351	0.46761	0.83108	6.27901	0.97497	0.84740
2.00	3.19416	0.47094	0.84781	6.75247	0.97765	0.86335
2.50	4.34959	0.48173	0.90292	9.02033	0.98619	0.91467
3.00	5.45464	0.48742	0.93257	11.19124	0.99058	0.94148
3.50	6.53058	0.49081	0.95042	13.31055	0.99315	0.95731
4.00	7.58805	0.49298	0.96200	15.39881	0.99479	0.96747

TABLE V. Extrapolated values of staggered magnetization, spin gap, and their ratio defined by Eq. (5) to the thermodynamic limit as a function of Δ for the $S = 1/2$ honeycomb-lattice XXZ Heisenberg model obtained by our DMRG calculations.

	$S = 1/2$			$S = 1$		
Δ	$\varepsilon_{\rm hon}(\frac{1}{2}, \Delta)$	$m^z_{\rm hon}(\frac{1}{2}, \Delta)$	$r_{\rm hon}(\frac{1}{2}, \Delta)$	$\varepsilon_{\rm hon}(1, \Delta)$	$m^z_{\rm hon}(1, \Delta)$	$r_{\rm hon}(1, \Delta)$
1.00	−0.01917	0.27637	−0.02312	−0.01448	0.75925	−0.00636
1.05	0.30264	0.31882	0.30135	0.77160	0.82632	0.29644
1.10	0.43473	0.34256	0.38456	1.14549	0.85580	0.40561
1.15	0.55835	0.35957	0.45010	1.46041	0.87559	0.48345
1.20	0.67549	0.37295	0.50312	1.73880	0.89047	0.54241
1.30	0.89595	0.39335	0.58403	2.24251	0.91197	0.63051
1.40	1.10423	0.40856	0.64351	2.69467	0.92701	0.69210
1.50	1.30397	0.42045	0.68919	3.11703	0.93819	0.73831
1.60	1.49774	0.43004	0.72558	3.51818	0.94683	0.77412
1.70	1.68690	0.43792	0.75531	3.90403	0.95368	0.80267
1.80	1.87243	0.44451	0.78007	4.27815	0.95924	0.82592
1.90	2.05486	0.45008	0.80097	4.64300	0.96381	0.84514
2.00	2.23472	0.45484	0.81887	5.00033	0.96764	0.86126
2.50	3.10562	0.47085	0.87944	6.71114	0.97988	0.91319
3.00	3.94431	0.47960	0.91379	8.34704	0.98624	0.94039
3.50	4.76235	0.48494	0.93529	9.94248	0.98997	0.95649
4.00	5.56612	0.48843	0.94967	11.51335	0.99237	0.96683

$S = 1$ [35]. Fitting our DMRG data within the range $0 \leqslant 1/\Delta \leqslant 0.02$ yields coefficients $m_2 = -1.852\,848\,25$ for $S = 1/2$ and $m_2 = 1.949\,925\,36$ for $S = 1$. These findings are in remarkable concordance with the established SE coefficients, further affirming the reliability of our DMRG computational approach.

APPENDIX D: SERIES EXPANSION FOR SPIN GAP IN THE $S = 1/2$ HONEYCOMB-LATTICE XXZ HEISENBERG MODEL

Around the classical limit, perturbative expansion up to the 10th order in $1/\Delta$ for the $S = 1/2$ honeycomb-lattice XXZ Heisenberg model yields the spin gap as

$$\varepsilon_{\rm hon}\left(\frac{1}{2}, \Delta\right) = \frac{3}{2} - \frac{15}{8\Delta^2} + \frac{2.304\,687\,5}{\Delta^4} - \frac{7.051\,025\,390\,62}{\Delta^6} + \frac{26.376\,685\,634\,7}{\Delta^8} - \frac{111.596\,182\,008}{\Delta^{10}}. \tag{D1}$$

We denote the results obtained by considering terms up to the nth order as SEn and plot them as a function of Δ in Fig. 10, alongside a comparison with our DMRG results. As indicated by Eq. (D1), the inclusion of higher-order terms introduces significant oscillations near $\Delta = 1$ due to the increasing coefficients of these terms. Consequently, within the region $\Delta \lesssim 2$, there is a noticeable deviation from the DMRG results. To approximate the DMRG findings even more closely, it is anticipated that a considerably higher order of terms must be accounted for, suggesting that the impact of quantum fluctuations on spin excitations is significant in this Néel phase.

APPENDIX E: DMRG DATA FOR STAGGERED MAGNETIZATION AND SPIN GAP

For additional context, we present the values of staggered magnetization and spin gap obtained via the DMRG method at the thermodynamic limit for various values of Δ. Tables IV and V detail these quantities for the square and honeycomb lattices, respectively. Moreover, the values of the ratio of staggered magnetization to the spin gap, as plotted in Fig. 9 of the main text, are also provided for reference.

[1] U. Schollwöck, J. Richter, D. J. Farnell, and R. F. Bishop, *Quantum Magnetism*, Lecture Notes in Physics Vol. 645 (Springer, New York, 2004).

[2] C. Lacroix, P. Mendels, and F. Mila, *Introduction to Frustrated Magnetism: Materials, Experiments, Theory* (Springer Science & Business Media, New York, 2011), Vol. 164.

[3] S. Sachdev, *Quantum Phase Transitions* (Cambridge University Press, Cambridge, 2011).

[4] W. Heisenberg, On the theory of ferromagnetism, Z. Phys. **49**, 619 (1928).

[5] M. E. Lines, Magnetic properties of $CoCl_2$ and $NiCl_2$, Phys. Rev. **131**, 546 (1963).

[6] N. Achiwa, Linear antiferromagnetic chains in hexagonal ABCl3-type compounds (A; Cs, or Rb, B; Cu, Ni, Co, or Fe), J. Phys. Soc. Jpn. **27**, 561 (1969).

[7] L. Savary and L. Balents, Quantum spin liquids: A review, Rep. Prog. Phys. **80**, 016502 (2017).

[8] Y. Zhou, K. Kanoda, and T.-K. Ng, Quantum spin liquid states, Rev. Mod. Phys. **89**, 025003 (2017).

[9] J. R. Schrieffer and J. S. Brooks, *Handbook of High-temperature Superconductivity: Theory and Experiment* (Springer, New York, 2007).

[10] B. A. Bernevig, T. L. Hughes, and S.-C. Zhang, Quantum spin Hall effect and topological phase transition in HgTe quantum wells, Science **314**, 1757 (2006).

[11] M. Kadosawa, M. Nakamura, Y. Ohta, and S. Nishimoto, One-dimensional projection of two-dimensional systems using spiral boundary conditions, Phys. Rev. B **107**, L081104 (2023).

[12] M. Kadosawa, M. Nakamura, Y. Ohta, and S. Nishimoto, Study of staggered magnetization in the spin-s square-lattice Heisenberg model using spiral boundary conditions, J. Phys. Soc. Jpn. **92**, 023701 (2023).

[13] K. Kubo and T. Kishi, Existence of long-range order in the XXZ model, Phys. Rev. Lett. **61**, 2585 (1988).

[14] Z. Weihong, J. Oitmaa, and C. J. Hamer, Second-order spin-wave results for the quantum XXZ and XY models with anisotropy, Phys. Rev. B **44**, 11869 (1991).

[15] V. S. Viswanath, S. Zhang, J. Stolze, and G. Müller, Ordering and fluctuations in the ground state of the one-dimensional and two-dimensional $S = 1/2$ XXZ antiferromagnets: A study of dynamical properties based on the recursion method, Phys. Rev. B **49**, 9702 (1994).

[16] S. Yunoki, Numerical study of the spin-flop transition in anisotropic spin-$\frac{1}{2}$ antiferromagnets, Phys. Rev. B **65**, 092402 (2002).

[17] B. Braiorr-Orrs, M. Weyrauch, and M. V. Rakov, Numerical studies of entanglement properties in one- and two-dimensional quantum Ising and XXZ models, Ukrain. J. Phys. **61**, 613 (2016).

[18] R. Bishop and P. Li, Large-s expansions for the low-energy parameters of the honeycomb-lattice Heisenberg antiferromagnet with spin quantum number s, J. Magn. Magn. Mater. **407**, 348 (2016).

[19] I. Affleck, T. Kennedy, E. H. Lieb, and H. Tasaki, Valence bond ground states in isotropic quantum antiferromagnets, Commun. Math. Phys. **115**, 477 (1988).

[20] J. Wojtkiewicz, K. Wohlfeld, and A. M. Oleś, Long-range order in the XY model on the honeycomb lattice, Phys. Rev. B **107**, 064409 (2023).

[21] M. Nakamura, S. Masuda, and S. Nishimoto, Characterization of topological insulators based on the electronic polarization with spiral boundary conditions, Phys. Rev. B **104**, L121114 (2021).

[22] S. R. White, Density matrix formulation for quantum renormalization groups, Phys. Rev. Lett. **69**, 2863 (1992).

[23] M. Kadosawa, M. Nakamura, Y. Ohta, and S. Nishimoto, Phase diagram of the Kitaev-Heisenberg model using various finite-size clusters, J. Phys. Soc. Jpn. **92**, 055001 (2023).

[24] R. R. P. Singh, Thermodynamic parameters of the $t = 0$, spin-1/2 square-lattice Heisenberg antiferromagnet, Phys. Rev. B **39**, 9760 (1989).

[25] R. R. P. Singh, Quantum renormalizations in the spin-1 Heisenberg antiferromagnet on the square lattice, Phys. Rev. B **41**, 4873 (1990).

[26] Z. Weihong, J. Oitmaa, and C. J. Hamer, Square-lattice Heisenberg antiferromagnet at $t = 0$, Phys. Rev. B **43**, 8321 (1991).

[27] R. Bishop, P. Li, R. Zinke, R. Darradi, J. Richter, D. Farnell, and J. Schulenburg, The spin-half XXZ antiferromagnet on the square lattice revisited: A high-order coupled cluster treatment, J. Magn. Magn. Mater. **428**, 178 (2017).

[28] C. J. Hamer, Z. Weihong, and P. Arndt, Third-order spin-wave theory for the Heisenberg antiferromagnet, Phys. Rev. B **46**, 6276 (1992).

[29] J.-i. Igarashi, $1/S$ expansion for thermodynamic quantities in a two-dimensional Heisenberg antiferromagnet at zero temperature, Phys. Rev. B **46**, 10763 (1992).

[30] C. M. Canali and M. Wallin, Spin-spin correlation functions for the square-lattice Heisenberg antiferromagnet at zero temperature, Phys. Rev. B **48**, 3264 (1993).

[31] S. R. White and A. L. Chernyshev, Neél order in square and triangular lattice Heisenberg models, Phys. Rev. Lett. **99**, 127004 (2007).

[32] I. Niesen and P. Corboz, Emergent Haldane phase in the $S = 1$ bilinear-biquadratic Heisenberg model on the square lattice, Phys. Rev. B **95**, 180404(R) (2017).

[33] A. W. Sandvik and H. G. Evertz, Loop updates for variational and projector quantum Monte Carlo simulations in the valence-bond basis, Phys. Rev. B **82**, 024407 (2010).

[34] D. A. Huse, Ground-state staggered magnetization of two-dimensional quantum Heisenberg antiferromagnets, Phys. Rev. B **37**, 2380 (1988).

[35] J. Oitmaa, C. J. Hamer, and Z. Weihong, Quantum magnets on the honeycomb and triangular lattices at $T = 0$, Phys. Rev. B **45**, 9834 (1992).

[36] R. Ganesh, J. van den Brink, and S. Nishimoto, Deconfined criticality in the frustrated Heisenberg honeycomb antiferromagnet, Phys. Rev. Lett. **110**, 127203 (2013).

[37] Z. Zhu, D. A. Huse, and S. R. White, Weak plaquette valence bond order in the $S = 1/2$ honeycomb J_1–J_2 Heisenberg model, Phys. Rev. Lett. **110**, 127205 (2013).

[38] S.-S. Gong, D. N. Sheng, O. I. Motrunich, and M. P. A. Fisher, Phase diagram of the spin-$\frac{1}{2}J_1 - J_2$ Heisenberg model on a honeycomb lattice, Phys. Rev. B **88**, 165138 (2013).

[39] E. V. Castro, N. M. R. Peres, K. S. D. Beach, and A. W. Sandvik, Site dilution of quantum spins in the honeycomb lattice, Phys. Rev. B **73**, 054422 (2006).

[40] A. F. Albuquerque, D. Schwandt, B. Hetényi, S. Capponi, M. Mambrini, and A. M. Läuchli, Phase diagram of a frustrated quantum antiferromagnet on the honeycomb lattice: Magnetic order versus valence-bond crystal formation, Phys. Rev. B **84**, 024406 (2011).

[41] C. J. Hamer, J. Oitmaa, and Z. Weihong, Zero-temperature properties of the quantum XY model with anisotropy, Phys. Rev. B **43**, 10789 (1991).

[42] H. L. Davis, New method for treating the antiferromagnetic ground state, Phys. Rev. **120**, 789 (1960).

[43] M. Parrinello and T. Arai, Infinite-order cumulant expansion for spins, Phys. Rev. B **10**, 265 (1974).